Article:
Al-Gailani, A orcid.org/0000-0001-9290-0636, Sanni, O orcid.org/0000-0002-3895-7532, Charpentier, TVJ et al. (3 more authors) (2020) Examining the effect of ionic constituents on crystallization fouling on heat transfer surfaces. International Journal of Heat and Mass Transfer, 160. 120180. ISSN 0017-9310

https://doi.org/10.1016/j.ijheatmasstransfer.2020.120180

Examining the Effect of Ionic Constituents on Crystallization Fouling on Heat Transfer Surfaces

Amthal Al-Gailani[1]*, Olujide Sanni[1], Thibaut V. J. Charpentier[2], Richard Crisp[3], Jantinus H. Bruins[4] and Anne Neville[1]

[1] *School of Mechanical Engineering, University of Leeds, Leeds, LS2 9JT, England*

[2]*School of Chemical and Process Engineering (SCAPE), University of Leeds, Leeds, LS2 9JT, England*

[3] *Fernox Limited, Woking, Surrey, GU21 5RW, England*

[4]*WLN, Glimmen, 9756 AD, Netherlands*

Abstract

The effect of the most abundant constituents in potable water on fouling of aluminium surface has been studied systematically in this work. The role of sodium, chloride, magnesium and sulphate ions and total organic carbon (TOC) on the fouling kinetics and morphology was assessed using a once-through open flow cell. The findings showed that the fouling resistance to heat transfer increases with the concentration of chloride and sodium. A complex influence of magnesium was found on the scaling process, varying between inhibition and promotion of scale formation depending on the concentration. At high concentrations of Mg^{2+}, the formed scale layer consists of needle-like aragonite coated by a crust of magnesium deposits. The inhibitory performance of sulphate SO_4^{2-} was found to be insignificant when compared with Mg^{2+} under similar conditions. Even though it is undesirable in potable water, inhibition efficiencies of TOC were 31.3% and 47.9% at concentrations of 2 and 4.3 mg/L respectively. The morphology observations illustrated that the presence of TOC produces a rough scale layer.

Keywords: Heat transfer, Fouling resistance, Domestic appliances, Aluminium, Magnesium, Calcium carbonate.

1.Introduction

Mineral scale formation on heat transfer surfaces associated with water heating processes is a complex problem that is often expensive to remedy. The formation of sparingly soluble inorganic deposits can impair the performance of household appliances such as boilers, steam irons, coffee makers washing machines, dishwashers and potable water distribution systems [1]. Surface deposition causes a reduction in heat transfer efficiency, increasing the power consumption and blockage of flowlines in domestic devices subjected to fouling [2-5]. The scaling process in these devices is distinguished by some unique

features including the heating to water boiling point, steaming and composite fouling layer of various elements [6].

A variety of ionic species exist in potable water, such as Ca^{2+}, Mg^{2+}, Na^{+}, Cl^{-}, HCO^{-} and SO_4^{2-} and it is well known that some of these can contribute positively or negatively to the scale layer growth rate [7, 8]. It has been demonstrated by Tai et al. [9] that the presence of sodium ions slightly influences the induction time of calcium carbonate ($CaCO_3$) formation in a semi-batch crystallizer. Similarly, it has been found that some monovalent cations have little influence on the fouling kinetics [10, 11]. However, it is difficult to exclude Cl^{-} from test solutions to investigate the effect of Na^{+} alone. It has long been known that chloride ions are aggressive towards many pipe materials by enhancing the corrosion rate [12]. The presence of Cl^{-} in potable water as a biocide may also potentially diminish the effectiveness of scale control additives such as poly-maleic acid that leads to a totally different response from these additives [13, 14].

The presence of magnesium in potable water could contribute towards either scaling reduction or promotion. Chen et al. [15] reported that Mg^{2+} suppressed the formation of $CaCO_3$ on surfaces and in the bulk solution through adsorption of Mg^{2+} on the active sites of the crystal which may increase the solubility of scale particles. It has also been observed that Mg^{2+} reduces the rate of calcite crystallization [16], and it increases the induction time by about 28 times [17]. On the other hand, solutions supersaturated with Mg^{2+} at high temperatures pose a potential formation of magnesium deposits such as magnesium carbonate ($MgCO_3$), magnesium oxide (MgO) and magnesium hydroxide (MgOH).

A few studies concerning the effect of SO_4^{2-} have focused on bulk precipitation. It has been found that the presence of SO_4^{2-} has a weak inhibitory effect on scale formation. However, at concentrations above 0.01 M, the transformation of calcite to aragonite is favourable. Sulphate ions preferably bind to calcite rather than aragonite [18, 19]. Waly et al. [17] reported that the induction time of the calcium carbonate formation in seawater reverse osmosis system has been increased by 11 times when adding 0.025 mol/L of SO_4^{2-}.

Natural organics exist in water from various sources. They are complex molecules which affect the colour, odour, taste and causing serious health issues. The predominant type of natural organic material is known as humic substances which are classified into humin, fulvic acids and humic acids [20, 21]. The solubility of humic acids, which is pH-dependent, raises the content of total organic carbon (TOC) in potable water. The typical molecular structure of humic acid is shown in Fig.1 [22]. The presence of TOC in water can inhibit the formation of inorganic scale [23, 24].

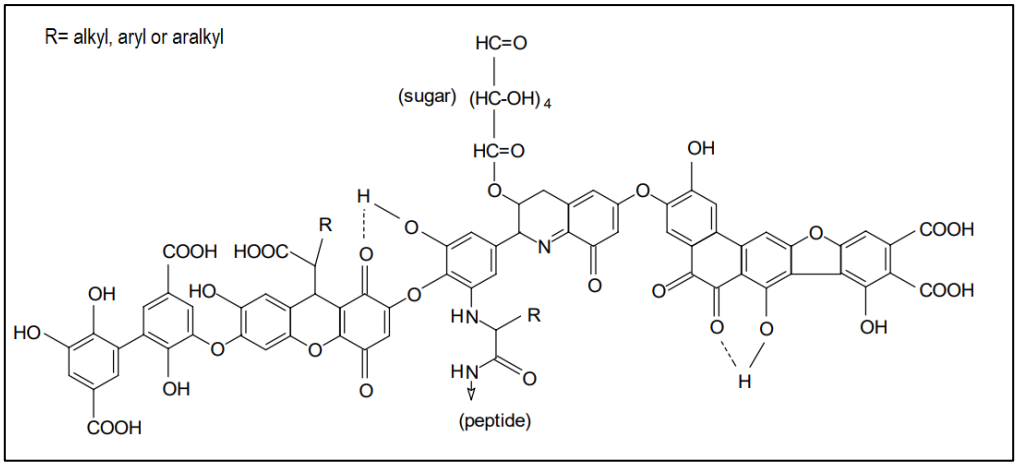

Fig.1. Model structure of the humic acid molecule according to Stevenson [25]

The fouling process in household systems is complex and it can be affected by different parameters as well as water chemistry. The presence of various ionic species in potable water complicates the understanding of fouling kinetics and deposit structure. The aim of this study, therefore, is to investigate the influence of potable water constituents namely; Mg^{2+}, Na^{+}, Cl^{-}, SO_4^{2-} and TOC on the scale formation kinetics at constant operating conditions. A study of the surface crystallization of inorganic scale from different solutions was carried out in a rectangular open flow channel. The deposit morphology on the heat transfer surface was simultaneously discussed.

2.Experimental methods

2.1.Test solution

The composition of solutions used in the present experiments is given in Table 1. Solution A is commercially-available bottled water with a pH of 7.2. It has been chosen for its hardness of 307 ppm of $CaCO_3$, which is almost same as potable water hardness in some areas the south UK. Solutions B-M and TOC-containing solutions are prepared in the laboratory using deionized water. All solutions have been filtered using 20-25 μm filter paper, and then a sample from each solution is taken to measure the initial value of pH and ion content.

Different grades of reagent salt are used in the preparation of the solutions (B-M); namely $CaCl_2.6H_2O$ (Purity: 97 to 100%) (Honeywell Fluka), Na_2SO_4 (Purity: min. 99%) (VWR Chemicals), $MgCl_2.6H_2O$ (Purity: 100%) (VWR Chemicals), $NaHCO_3$ (Purity: 99.5%) (ACROS Organics) and NaCl (purity: min. 99%) (Honeywell Fluka). 167 mg of sodium chloride NaCl was dissolved in solution B to increase the concentrations of chloride to 315 mg/L and sodium to 202 mg/L in solution C. Humic acid (Sigma Aldrich) was used to prepare TOC-containing solutions. The humic acid powder was dissolved to solution B after pH change to 12.

The solutions used to determine the effect of TOC on the scale formation are not listed in Table 1. The humic acid solubility is pH-dependent, as such, the pH of deionized water was raised to 12 by adding 3 ml of NaOH solution (50 wt. %) to each litre of water. 26 and 9.75 mg/L of humic acid was dissolved using a magnetic stir bar at a rate of 600 rpm to obtain a TOC concentration of 4.3 and 2 mg/L, respectively. As the inorganic carbonate formation is favoured at high pH values, the pH of the humic acid solution was lowered to 7 using 2.5 ml of HCl (20 vol. %) solution. Based on the corrected volume of the humic acid solution, salts $CaCl_2.6H_2O$, Na_2SO_4, $NaHCO_3$ and $MgCl_2.6H_2O$ were dissolved at the same mixing rate to achieve the same composition of solution B.

Table 1. Solution compositions.

Elements, mg/L	$[Ca^{2+}]$	$[Mg^{2+}]$	$[HCO_3^-]$	$[SO_4^{2-}]$	$[Cl^-]$	$[Na^+]$
Solution A	80	26	360	14	10	6.5
Solution B	80	26	360	14	216	136
Solution C	80	26	360	14	315	202
Solution D	80	0	360	14	140	136
Solution E	80	52	360	14	292	136
Solution F	80	104	360	14	443	136
Solution G	80	150	360	14	577	136
Solution H	80	0	360	0	140	130
Solution I	0	26	360	0	75	130
Solution J	0	80	360	0	233	130
Solution K	80	26	360	42	216	149
Solution L	80	26	360	126	216	188
Solution M	80	26	360	0	216	130

2.2.Experimental setup and procedure

The schematic view of the experimental apparatus is shown in Fig. 2. It consists of a solution tank, peristaltic pump, test flow cell, sample heating system, data acquisition system and waste tank. This once-through flow system was adopted to avoid any reduction in the saturation state which may result from solution re-circulation. The flow cell (cell volume of 400 ml), where surface scale deposits, is designed to work under atmospheric pressure with open top window (Fig. 3). The outer body part is made of nylon 6 (130 mm length, 50 mm wide and 55 mm height) with 10 mm wall thickness. In the middle, a metal sample is fixed by a sample holder made of nylon 6. The cell has three inlets and six

outlets positioned at different height levels from the base to regulate or change the level of solutions in the cell when required.

The solution is pumped from the solution tank into the flow cell with a digital peristaltic pump at a controlled flow rate. In the cell, the solution flows over the metal sample in a laminar regime with no fluid recirculation. As the initial surface temperature of the sample is 100 ºC in all the experiments, the solution partially evaporates, and the steam leaves the cell through the upper open window while the remaining solution leaves the cell to the waste tank. For all experiments, the flow rate and initial surface temperature were set at 8 ml.min^{-1} and 100± 1 ºC, respectively.

The metallic cylindrical sample was made of aluminium with dimensions of 22 mm in height and 20 mm outer diameter. Aluminium was selected as it is one of the most commonly used materials in constructing pipes, pools and household appliances. The sample was configured to be a one-sided hollow cylinder with an inner diameter of 6.7 mm (Fig. 4). The cavity enables the position of a cartridge heater for heating the sample. A 3 mm depth channel was made in an internal wall to fix the temperature probe between the heater and sample. The top surface of the sample, which is the tested surface, was grinded with silicon carbide paper (1200 grit) and then polished with diamond suspension (0.5 µm) by a mechanical polishing method. It was subsequently rinsed with acetone, distilled water and dried at 37 ºC for 24 hours.

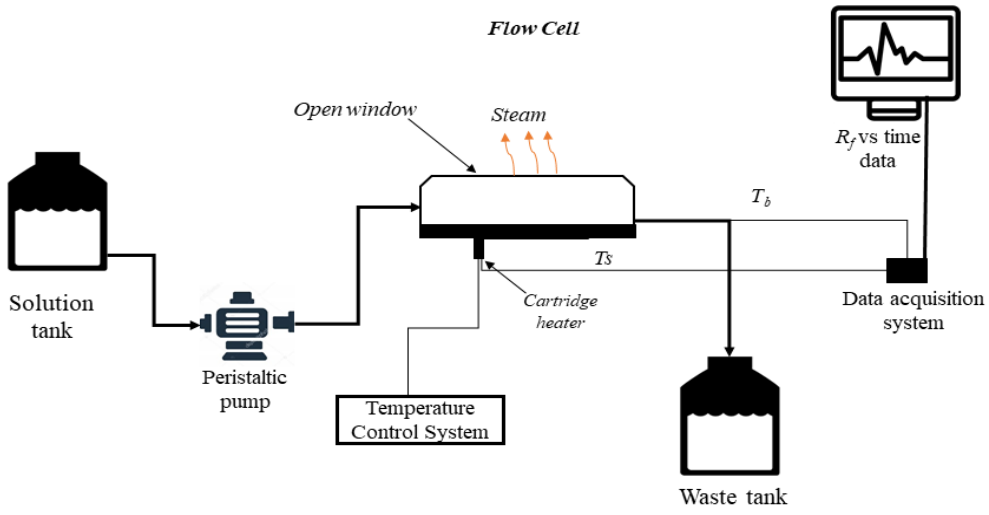

Fig. 2. Configuration of the experimental apparatus.

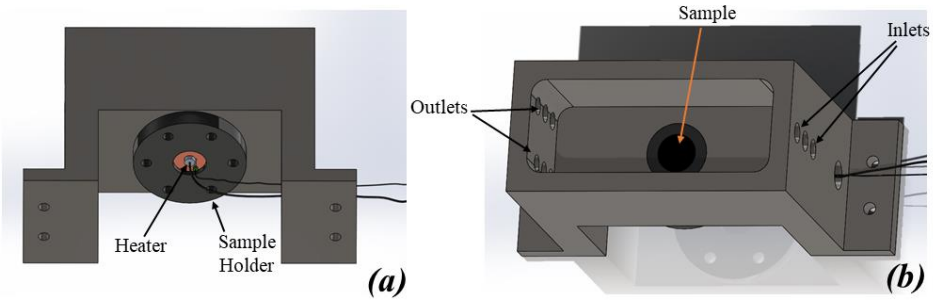

Fig. 3. The flow cell; (a) bottom view and (b) top view.

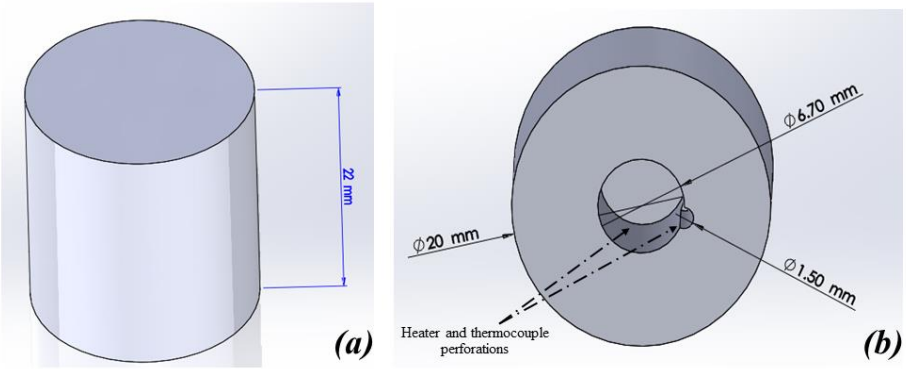

Fig. 4. The aluminium; (a) Top view and (b) Bottom view.

The influence of the resistive fouling layer on the heat transfer was evaluated using fouling resistance. The growth of the scale layer leads to an increase in the surface temperature and a reduction of the bulk temperature. Three mineral-insulated thermocouple sensors were used to measure the surface and bulk temperatures. These sensors were attached to a data acquisition system in which the analogue signals are converted into digital numeric values that are subsequently stored automatically. Fouling resistance (R_f) was calculated using the analytical expressions for convection heat transfer [26]:

$$R_f = \frac{1}{U_f} - \frac{1}{U_c} \quad \textbf{(1)}$$

$$R_f = \left(\frac{T_w - T_b}{Q}\right)_f - \left(\frac{T_w - T_b}{Q}\right)_c \quad \textbf{(2)}$$

$$R_f = \frac{T_w^f - T_w^c - T_b^f - T_b^c}{Q} \quad \textbf{(3)}$$

Where, U_f is the overall heat transfer coefficient for the fouled surface, U_c is the overall heat transfer coefficient for the clean surface, Q is the heat flux, T_w is the surface temperature, T_b is the bulk temperature, superscript *f* is for fouled surface and *c* is for a clean surface. It is very difficult to measure the bulk temperature at a certain point within the cell, as such the average value of the inlet and outlet temperatures is considered. The fourth temperature sensor was fixed between the heater and sample to send feedback to the heating system which controls the temperature with an accuracy of ± 1 ℃. The heating system generates the required heat flux to heat the surface using a cartridge heater (L: 25 mm,

OD: 6.5 mm and power: 150 W). The heat flux, *Q,* was measured using a plug-in power monitor (Primera, Brennenstuhl).

The techniques used to analyse the surface and solution are divided into pre-test and post-test analysis techniques. Prior to an experiment, the roughness of the top surface of the dried sample was examined using the 3D optical profiler NPFlex (Bruker, USA). The arithmetic average of the absolute values of the surface roughness (R_a) was kept between 21.8 to 34 nm in all tests. The sample weight, before and after the test, was determined using a digital laboratory balance (Oxford GM2505D) with an accuracy of ± 1.5 mg. Regarding the test solutions, the initial concentration of the divalent cations in water and pH was measured using atomic absorption spectrophotometer (*AAS*) (Agilent Technologies, USA) and HI 8014 Hanna pH-meter, respectively. The concentration of total organic carbon (TOC) was measured by Hach-Lange IL550 analyser (Hach Lange Ltd, UK). For the post experiment, the scaled surface is rinsed with deionized water and then dried in an oven at 37 ºC for 24 hours. The Scanning Electron Microscope SEM (Carl Zeiss EVO MA15) was used for investigating the habit of the deposit crystals. Energy dispersive X-ray (EDX) elemental analysis was used to determine the composition of scale particles. Crystalline structures of the fouling layer were analysed by Philips X'Pert X-ray diffractometer (Cu anode x-ray source) with the 2 theta between 20 to 60º. The standard deviation of arithmetic mean value for at least two repeats was calculated for the experimental error bars.

3. Results and Discussion

3.1. Effect of sodium and chloride ions

The fouling resistance to heat transfer and the mass of scale formed from solutions with different contents of sodium and chloride are presented in Fig.5a and 5b. It can be seen that the fouling resistance increases with the content of chloride and sodium ions. The kinetics of scale formation is enhanced as the concentrations of chloride and sodium ions increase. However, it has been reported that the sodium ion has no inhibitory effect on crystal growth or morphology [9]. The dissociation constant of bicarbonate HCO_3^- to carbonate CO_3^{2-} changes as a function of solution temperature and salinity [27, 28]. Increase in chloride ion (Cl^-) content enhances the solution salinity and the dissociation constant of bicarbonate ion, hence higher amount of carbonate is produced and more calcium carbonate and magnesium carbonate deposit on the surface.

In terms of deposit morphology, some changes have been observed as the concentration of chloride and sodium ions increase (Fig. 6). The needle-like aragonite is the dominant polymorphic phase in all tested solutions. However, it can be observed that the needles formed from solution A are larger when compared with those formed from solutions B and C. The SEM image in Fig. 6b shows small holes distributed on the scale layer for the steam bubbles to leave the heated surface.

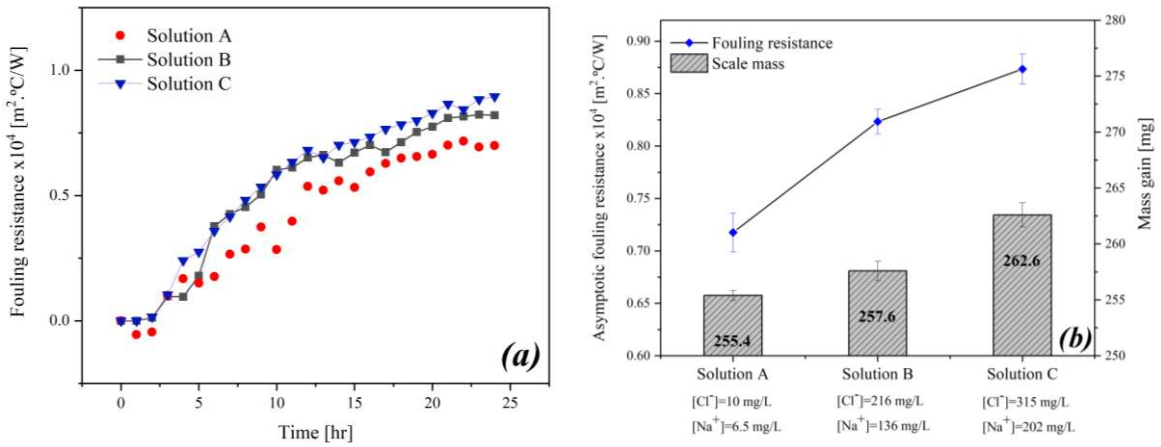

Fig. 5. (a) Thermal fouling resistance of scale on the aluminium surface, (b) surface mass gain and asymptotic fouling resistance, for different contents of chloride and sodium.

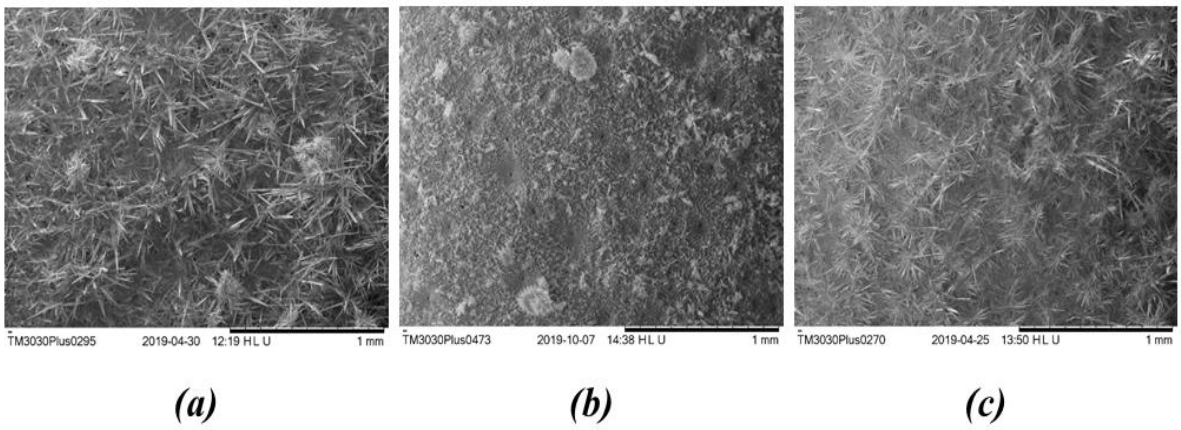

Fig 6. SEM image for deposits on the aluminium surface from different solutions; (a) solution A, (b) solution B and (c) solution C.

3.2. Effect of the magnesium ion

The effect of the concentration of magnesium ion on the thermal fouling resistance is shown in Fig. 7a and b. The solution with no magnesium ion produces a fouling layer with the highest insulation effect. Increasing the content of the magnesium ions from 26 to 104 mg/L reduces the resistance to heat transfer by 3.5 times. The Mg^{2+} poses inhibition influence on the formation of calcium carbonate which has been confirmed by Compton et al. [29] and Tai et al. [9]. It is found that the Mg^{2+} acted as an inhibitor through retarding the growth rate and/or incorporating into a crystal.

The fouling resistance increases again when the concentration of magnesium ion is increased to 150 mg/L. The increase of the saturation ratio of magnesium carbonate to about 60 provides enough driving force for the $MgCO_3$ scale to form. The formation of $MgCO_3$ besides $CaCO_3$ enhances the thermal fouling resistance to heat transfer. However, the concentration of chloride ion in solution G, 577 mg/L is the highest for all the solutions which, could also account for the increase in the fouling resistance by producing more carbonate from bicarbonate.

The SEM images in Fig. 8 show the changes that occurred when the concentration of Mg^{2+} increased to 150 mg/L. At a concentration of 52 mg/L, the scale particles are relatively small, and the overall layer is fluffy.

At 150 mg/L Mg^{2+}, a crust appears to cover the original aragonite crystal. This crust makes the needles in flower-like structures look thicker with a tapered end. The elemental analysis carried out by EDX shows that the content of magnesium ion in these needles is high as 32.7 wt. % with a small amount of calcium (Fig. 9). The presence of magnesium carbonate as magnesite and magnesium oxide as periclase is confirmed by the XRD analysis for the 150 mg/L Mg^{2+} sample. Aragonite is the only form of calcium carbonate that formed. Therefore, the formation of magnesium scales on the aragonite needles may increase the insulation capacity to the fouling layer.

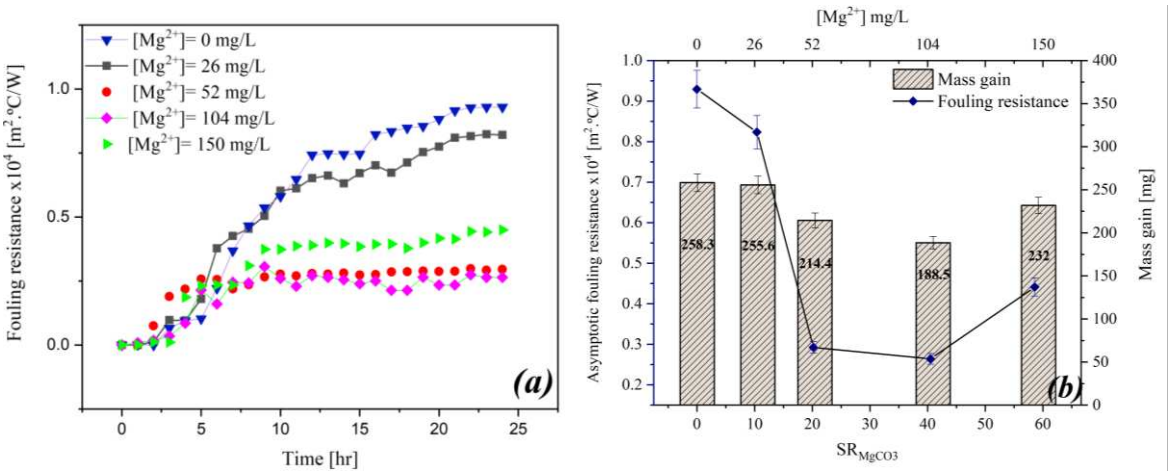

Fig. 7. (a) Thermal fouling resistance of scale on the aluminium surface, (b) surface mass gain and asymptotic fouling resistance, for different saturation ratios of $MgCO_3$.

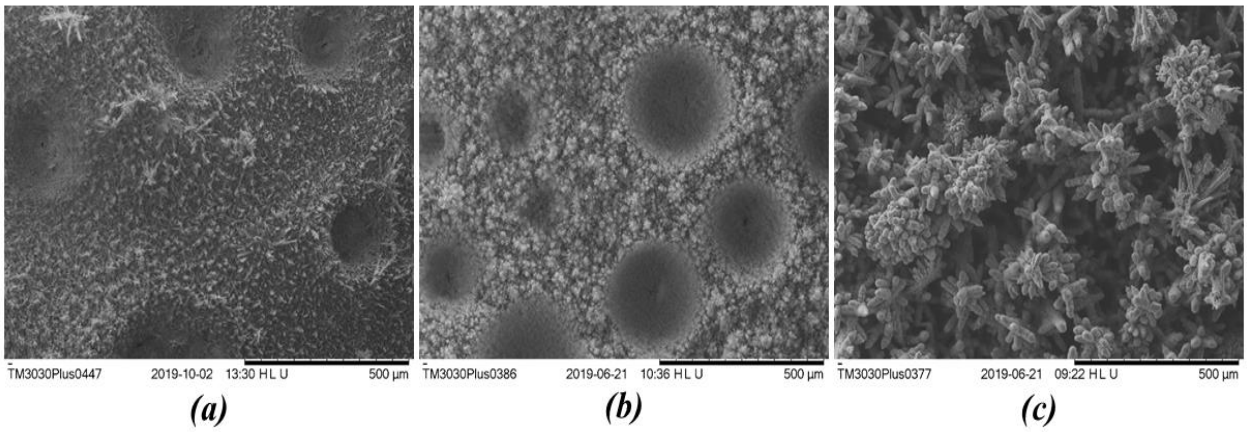

Fig 8. SEM image for deposits on the aluminium surface for different contents of magnesium; (a) no Mg^{2+}, (b) [Mg^{2+}] = 52 mg/L and (c) [Mg^{2+}] = 150 mg/L.

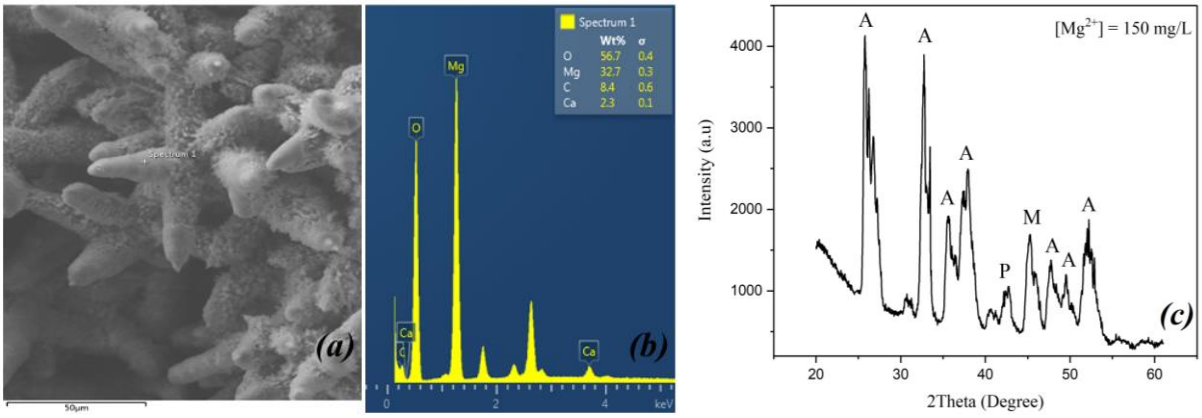

Fig. 9. EDX elemental analysis of the deposits on aluminium; (a) SEM image, (b) spectrum 1 and (c) XRD analysis of fouling layer at [Mg^{2+}] =150 mg/L, A for calcium carbonate as aragonite, M for magnesium carbonate as magnesite and P for magnesium oxide as periclase.

The fouling reaction from different divalent cations with carbonate (CO_3^{2-}) systems has been examined as shown in Fig. 10. The scale layer formed from the Ca^{2+}-CO_3^{2-} system (solution H) has higher thermal resistance than that formed from Mg^{2+}-CO_3^{2-} equilibrium systems (solutions I and J). For the same concentration in solutions H and J, Ca^{2+} and Mg^{2+} react separately with 360 mg/L of $HCO3^-$. The $CaCO_3$ deposits have a higher fouling resistance and the higher mass of 266.3 mg, while 72 mg for $MgCO_3$ scale. Under similar conditions, the reaction rate of calcium carbonate is greater than that of magnesium carbonate. However, the solubilities of both salts are close under the test temperature.

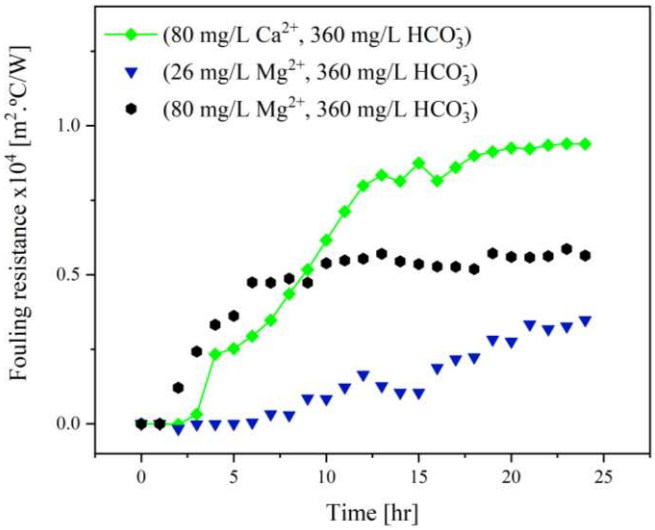

Fig. 10. Thermal fouling resistance of deposits on the aluminium surface for Mg^{2+}-CO_3^{2-} system (Solutions I and J) and Ca^{2+}-CO_3^{2-} systems (Solution H)

The SEM images in Fig. 11 show the scale structure from each solution. The calcium carbonate scale is a compact layer that consists mainly of aragonite needles (Fig.11a). However, it has been reported that

aragonite is a thermodynamically unstable phase of $CaCO_3$ at a temperature of 100 ºC [30]. As the scale is multi-layered, the first layer next to the surface might be calcite and the following layers are aragonite as the interface temperature decreases with each layer forms. Using solution I as scaling fluid produces a loose layer of small spherical crystals. Good agreement has been obtained between the present structure and the one reported by Raza et al. [31]. The increase of Mg^{2+} concentration to 80 mg/L generates a uniform crust of interlocking threads.

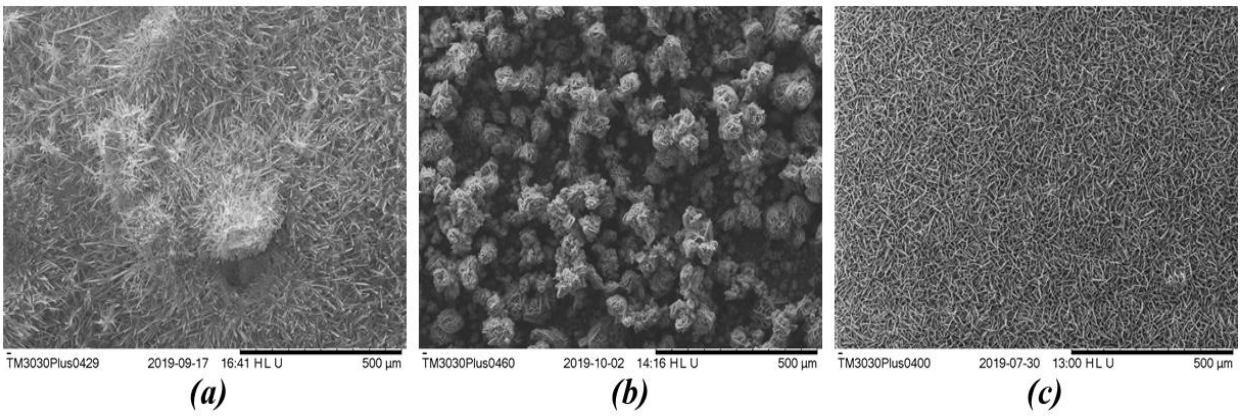

Fig 11. SEM image for deposits on the aluminium surface for Mg^{2+}-CO_3^{2-} and Ca^{2+}-CO_3^{2-} systems; (a) solution H, (b) solution I and (c) solution J.

3.3. Effect of sulphate ion

Change in the concentration of sulphate ion in drinking water has no significant influence on the insulation of inorganic deposits. The increase of SO_4^{2-} content in water slightly reduces the thermal fouling resistance (Fig. 12). It can be seen that there is no progress as the content of SO_4^{2-} increases from 42 to 126 mg/L (solutions A, J, K and L). In accordance with the literature, the inhibitory efficiency of sulphate ion is relatively small [18]. As the sulphate is one of the common fouling species, it is expected to support the fouling layer with calcium sulphate particles. However, neither the test temperature nor sulphate concentration is enough to supersaturate the solution. The solubility of calcium sulphate also is high in comparison with calcium carbonate and magnesium carbonate.

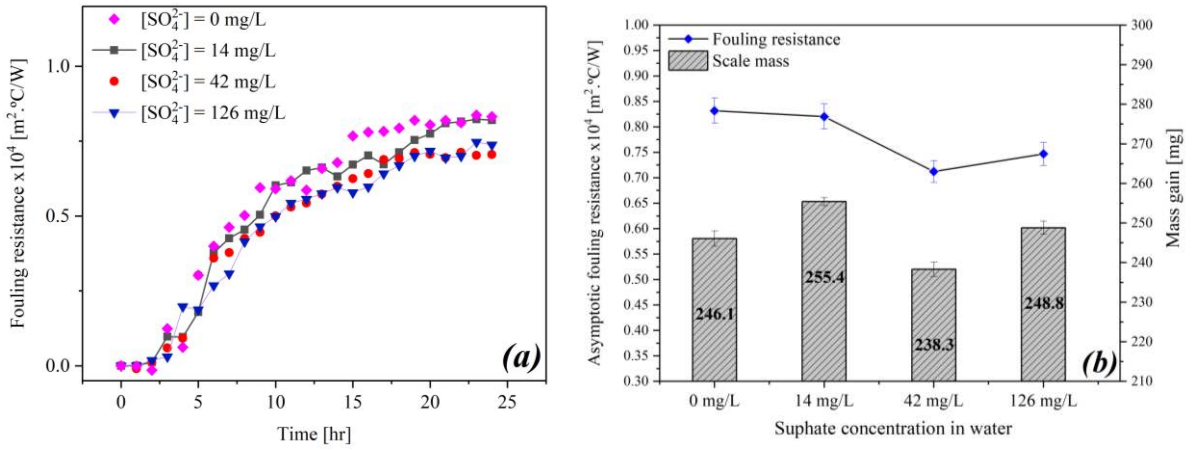

Fig. 12. (a) Thermal fouling resistance of scale on the aluminium surface, (b) surface mass gain and asymptotic fouling resistance, for different contents of sulphate in water.

In terms of the effect of sulphate ions on the morphology, SEM images are displayed in Fig. 13. The first image (Fig. 13a) shows the scale layer without the presence of sulphate ions in water. It looks like aragonite needles mixed with fluffy soft deposits. Then, it can be observed from the second image (fig. 13b), when the SO_4^{2-} content is 42 mg/L, that fouling layer consists of obvious plateaus of flower-like aragonite. Increasing the SO_4^{2-} content to 126 mg/L produces a plane crust of needle-like aragonite as shown in Fig. 13b. The presence of sulphate ions in water contributes to forming one crystal type of aragonite with even growth in all directions.

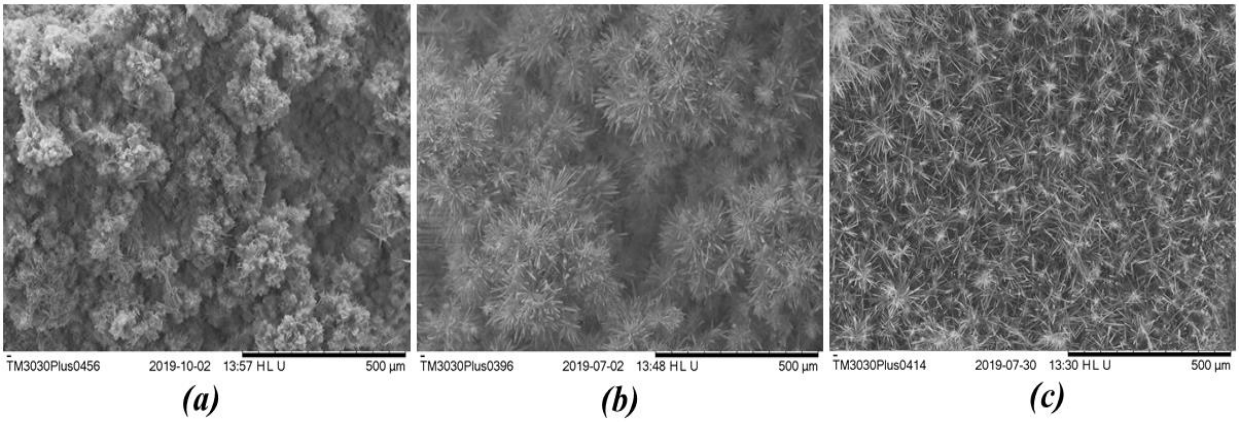

Fig 13. SEM image for deposits on aluminium surface for different concentrations of sulphate ion; (a) no sulphate, (b) $[SO_4^{2-}]$ = 42 mg/L and (c) $[SO_4^{2-}]$ = 126 mg/L

3.4. Effect of Total Organic Carbon (TOC)

The change of fouling resistance as a function of time in the presence of organic carbon (OC) in the solution is shown in Fig. 14a. The fouling resistance has been reduced by about 4 times when the TOC content increased to 2 mg/L. However, a further increase of TOC under the same experimental conditions does not pose a difference in the scale insulation effect. The molecule of humic acid, the

humic substance used to raise the TOC content, is relatively large (high molecular weight). It has been proposed by Hoch et al. [32] that the substances with high molecular weight generate a great reduction in growth rate. These molecules form a colloid/complex with Ca^{2+} and Mg^{2+} which lowers the saturation state and inhibits the growth of the crystal. The cations complexation is likely to occur by carboxylic acid and phenolic fictional groups [33].

The inhibition efficiencies of 31.3% and 47.9% are obtained for 2 and 4.3 mg/L of TOC respectively (Eq. 4). Evidently, at 2 mg/L TOC, the fouling resistance reduced much more than that at 4.3 mg/L. This might be explained as the TOC amount in water exceeds the amount required to inhibit the total surface deposition. Further increase in the amount of TOC accordingly does not contribute to a substantial reduction in scale formation. The amount of TOC needed to inhibit the fouling is subject to the operating conditions and water quality.

$$\% \text{ Inhibition efficiency} = \frac{M_a - M_p}{M_a} * 100 \qquad \textbf{(4)}$$

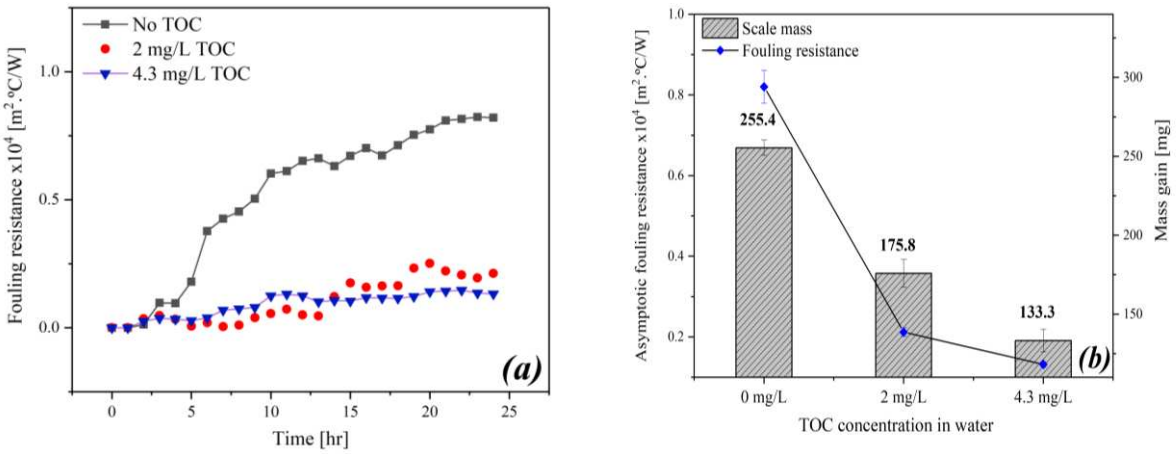

Fig. 14. (a) Thermal fouling resistance of scale on the aluminium surface and (b) surface mass gain and asymptotic fouling resistance, for different contents of TOC in water.

The inhibition role of the OC on the scale formation can be evaluated based on the morphology of the deposits. Fig.15. shows the effect of TOC content on the scale structure and morphology. The addition of 2 mg/L of TOC to the test solution produces a bumpy fouling layer with the non-uniform shape of crystals. By increasing the TOC content to 4.3 mg/L, the same structure is formed except for the appearance of some flat spots. Besides the formation of organics-Ca^{2+} complex, the aragonite crystals might be poisoned by OC in water yielding the presence scale layer. The TOC in the present experiments was high enough to react with all formed crystals. At the final stages of the fouling process, the removal and deposition rate become equal due to the weakness of the upper fouling sub-layer. Therefore, asymptotic fouling behaviour is observed in all fouling resistance graphs [34].

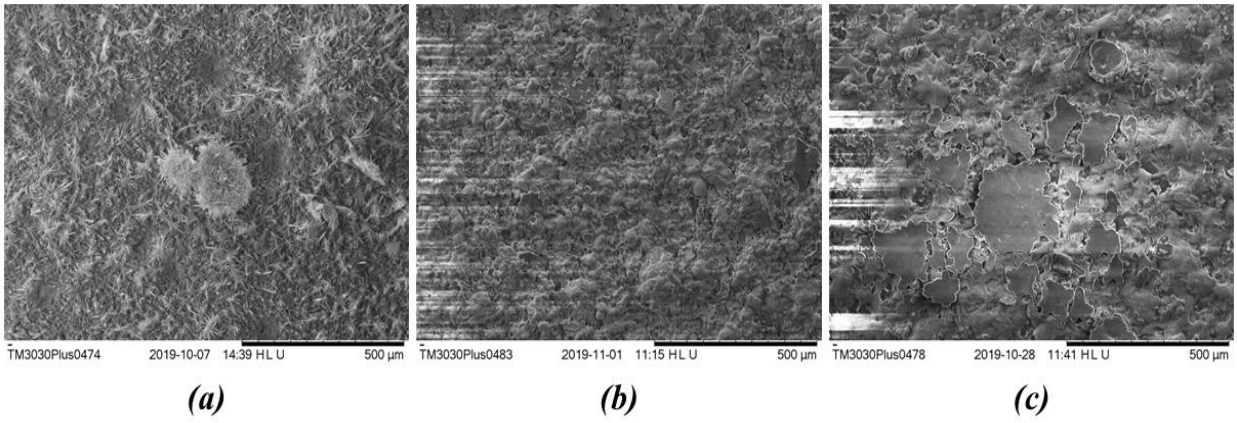

Fig 15. SEM image for deposits on aluminium surface for different concentrations of TOC; (a) no TOC, (b) [TOC] = 2 mg/L and (c) [TOC] = 4.3 mg/L.

The fouling of heat transfer surface has been evaluated using thermal fouling resistance, a mass of the fouling layer and SEM observations. Formation of different inorganic salts is expected on the heated surface which may lead to variation in some properties such as thermal conductivity and density of the fouling layer. Therefore, evaluating and comparing the fouling resistance with the mass of a fouling layer gives a good indication of how conductive the layer is. For instance, the increase of a foulant concentration in a solution may increase the fouling resistance with an insignificant change in the mass of deposits. as such, it can be concluded that the formed scale layer has less conductivity. The SEM images provide a piece of information about crystal size, morphology and fouling layer porosity which to further validate the findings from the fouling resistance and mass measurements.

4. Conclusions

This study has presented the surface deposition kinetics of inorganic scale in household systems from aqueous solution with different elemental contents. A series of laboratory-scale tests have been performed to mimic the fouling process in domestic appliances that use potable water from various sources, under atmospheric pressure. The deposit morphology was also studied using SEM, EDX and XRD techniques. The findings showed that the increase of chloride and sodium in potable water enhances the fouling rate and the deposited amount of scale on the heated surfaces. However, no remarkable change in the scale morphology has been marked as the content of chloride and sodium increase.

The presence of different concentrations of magnesium in water showed that there is no trend in the inhibition of scale formation. The increase of magnesium ion concentration from 26 to 104 mg/L reduces the resistance to heat transfer by about 3.5 times. However, increasing the [Mg^{2+}] to 150 mg/L enhances the fouling resistance. The SEM images showed that the needle-like aragonite is the dominant form of $CaCO_3$, the fouling layer is nevertheless fluffier at [Mg^{2+}] of 52 mg/L than that with no magnesium. At 150 mg/L Mg^{2+} looks like a crust covers the original aragonite needle. The EDX

findings showed that the content of magnesium in these coated needles is high as 32.7 wt. % with low abundance of calcium.

SO_4^{2-} ions have a minor inhibiting effect on the surface deposition. The fouling resistance has insignificantly reduced when the content of sulphate ions increased from 42 to 126 mg/L. Adding sulphate ions to water produces a less fluffy and structured layer of aragonite. Total organic carbon (TOC) at a concentration of 2 mg/L has reduced the fouling resistance to heat transfer by about 4 times. However, a further increase of TOC content does not pose a difference in the asymptotic fouling resistance which is owing to exceeding the TOC content the maximum concentration required to inhibit the entire surface deposition. The findings of morphology analysis illustrated that the presence of TOC poisons the scale crystals and deposits was transformed into a bumpy structure. These findings could be linked to the influence of the key operating conditions for a full understanding of the fouling process in household devices.

Acknowledgement

The authors acknowledge the funding and support from the Leeds University SALSAS consortium. We also acknowledge the financial support of the Leverhulme Trust Research Grant ECF-2016-204. We also wish to acknowledge the technical and administrative team of the Institute of Functional Surfaces (IFS), School of Mechanical Engineering at the University of Leeds for their supports.

Nomenclature

R	fouling resistance (m^2. K/W)
U	overall heat transfer coefficient (W m^{-2} K^{-1})
T	temperature (K)
Q	heat flux (W/m^2)
M	mass of scale (mg)

Acronyms

SEM	Scanning Electron Microscopy
XRD	X-ray Diffraction
EDX	Energy Dispersive X-ray
AAS	Atomic Absorption Spectrophotometry

Subscript/superscript

f	fouled surface
c	clean surface
w	surface/ wall
b	bulk
a	absence of TOC
p	presence of TOC

References

1. Richards, C.S., et al., *A 21st-Century Perspective on Calcium Carbonate Formation in Potable Water Systems.* Environmental Engineering Science, 2018. **35**(3): p. 143-158.
2. Zhao, J., et al., *A review of heterogeneous nucleation of calcium carbonate and control strategies for scale formation in multi-stage flash (MSF) desalination plants.* Desalination, 2018. **442**: p. 75-88.
3. Neville, A., *Surface Scaling in the Oil and Gas Sector: Understanding the Process and Means of Management.* Energy & Fuels, 2012. **26**(7): p. 4158-4166.
4. Sanni, O.S., et al., *Evaluation of laboratory techniques for assessing scale inhibition efficiency.* Journal of Petroleum Science and Engineering, 2019: p. 106347.
5. Al-Gailani, A., et al., *Inorganic mineral precipitation from potable water on heat transfer surfaces.* Journal of Crystal Growth, 2020. **537**: p. 125621.
6. Song, K.S., et al., *Composite fouling characteristics of CaCO3 and CaSO4 in plate heat exchangers at various operating and geometric conditions.* International Journal of Heat and Mass Transfer, 2019. **136**: p. 555-562.
7. MacAdam, J. and S.A. Parsons, *Calcium carbonate scale formation and control.* Re/Views in Environmental Science & Bio/Technology, 2004. **3**(2): p. 159-169.
8. Sano, Y. and D. Nakashima, *Prevention of calcium carbonate scale using electrolyzed water.* International Journal of Heat and Mass Transfer, 2018. **127**: p. 1147-1156.
9. Tai, C.Y. and W.-C. Chien, *Effects of operating variables on the induction period of CaCl2–Na2CO3 system.* Journal of crystal growth, 2002. **237**: p. 2142-2147.
10. Wada, N., K. Yamashita, and T. Umegaki, *Effects of silver, aluminum, and chrome ions on the polymorphic formation of calcium carbonate under conditions of double diffusion.* Journal of colloid and interface science, 1998. **201**(1): p. 1-6.
11. Söhnel, O. and J.W. Mullin, *Interpretation of crystallization induction periods.* Journal of colloid and interface science, 1988. **123**(1): p. 43-50.
12. Nalepa, C., et al., *A Comparison of Bromine-Based Biocides in a Medium Size Cooling Tower.* CTI JOURNAL, 1999. **20**: p. 42-61.
13. Li, H., et al., *Control of mineral scale deposition in cooling systems using secondary-treated municipal wastewater.* Water research, 2011. **45**(2): p. 748-760.
14. Dalvi, A.G.I., et al., *Role of chemical constituents in recycle brine on the performance of scale control additives in MSF plants.* Desalination, 2000. **129**(2): p. 173-186.
15. Chen, T., A. Neville, and M. Yuan, *Assessing the effect of Mg2+ on CaCO3 scale formation–bulk precipitation and surface deposition.* Journal of Crystal Growth, 2005. **275**(1-2): p. e1341-e1347.

16. Reddy, M.M. and K.K. Wang, *Crystallization of calcium carbonate in the presence of metal ions: I. Inhibition by magnesium ion at pH 8.8 and 25 C.* Journal of Crystal Growth, 1980. **50**(2): p. 470-480.
17. Waly, T., et al., *The role of inorganic ions in the calcium carbonate scaling of seawater reverse osmosis systems.* Desalination, 2012. **284**: p. 279-287.
18. Meyer, H., *The influence of impurities on the growth rate of calcite.* Journal of Crystal Growth, 1984. **66**(3): p. 639-646.
19. Østvold, T. and P. Randhol, *Kinetics of CaCO3 Scale Formation. The Influence of Temperature, Supersaturation and Ionic Composition*, in *International Symposium on Oilfield Scale*. 2001, Society of Petroleum Engineers: Aberdeen, United Kingdom. p. 9.
20. Aoustin, E., et al., *Ultrafiltration of natural organic matter.* Separation and Purification Technology, 2001. **22**: p. 63-78.
21. Zularisam, A., A. Ismail, and R. Salim, *Behaviours of natural organic matter in membrane filtration for surface water treatment—a review.* Desalination, 2006. **194**(1-3): p. 211-231.
22. Peña-Méndez, E.M., J. Havel, and J. Patočka, *Humic substances–compounds of still unknown structure: applications in agriculture, industry, environment, and biomedicine.* J. Appl. Biomed, 2005. **3**(1): p. 13-24.
23. Reddy, M.M. and A.R. Hoch, *Calcite crystal growth rate inhibition by aquatic humic substances*, in *Advances in crystal growth inhibition technologies*. 2002, Springer. p. 107-121.
24. Alvarez, R., et al., *Effects of humic material on the precipitation of calcium phosphate.* Geoderma, 2004. **118**(3): p. 245-260.
25. Stevenson, F.J., *Humus chemistry: genesis, composition, reactions*. 1994: John Wiley & Sons.
26. Krause, S., *Fouling of heat-transfer surfaces by crystallization and sedimentation.* International Chemical Engineering (A Quarterly Journal of Translations from Russia, Eastern Europe and Asia);(United States), 1993. **33**(3).
27. Prieto, F.J.M. and F.J. Millero, *The values of pK1+ pK2 for the dissociation of carbonic acid in seawater.* Geochimica et Cosmochimica Acta, 2002. **66**(14): p. 2529-2540.
28. Millero, F.J. and R.N. Roy, *A chemical equilibrium model for the carbonate system in natural waters.* Croatica chemica acta, 1997. **70**(1): p. 1-38.
29. Compton, R.G. and C.A. Brown, *The inhibition of calcite dissolution/precipitation: Mg2+ cations.* Journal of colloid and interface science, 1994. **165**(2): p. 445-449.
30. Ogino, T., T. Suzuki, and K. Sawada, *The formation and transformation mechanism of calcium carbonate in water.* Geochimica et Cosmochimica Acta, 1987. **51**(10): p. 2757-2767.
31. Raza, N., et al., *Leaching of natural magnesite ore in succinic acid solutions.* International Journal of Mineral Processing, 2015. **139**: p. 25-30.

32. Hoch, A.R., M.M. Reddy, and G.R. Aiken, *Calcite crystal growth inhibition by humic substances with emphasis on hydrophobic acids from the Florida Everglades.* Geochimica et Cosmochimica Acta, 2000. **64**(1): p. 61-72.
33. Fan, L., et al., *Influence of the characteristics of natural organic matter on the fouling of microfiltration membranes.* Water Research, 2001. **35**(18): p. 4455-4463.
34. Mayer, M., W. Augustin, and S. Scholl, *An approach to modeling induction period in crystallization fouling.* Heat and Mass Transfer, 2013. **49**(10): p. 1419-1432.